



Dust color temperature distribution of two FIR cavities at IRIS and AKARI maps

A. K. JHA and B. ARYAL* 

Central Department of Physics, Tribhuvan University, Kirtipur, Nepal.

*Corresponding author. E-mails: binil.aryal@uibk.ac.at; baryal@tucdp.edu.np

MS received 15 June 2017; accepted 20 December 2017; published online 6 March 2018

Abstract. By systematically searching the region of far infrared loops, we found a number of huge cavity-like dust structures at $60\ \mu\text{m}$ and $100\ \mu\text{m}$ IRIS maps. By checking these with AKARI maps ($90\ \mu\text{m}$ and $140\ \mu\text{m}$), two new cavity-like structures (sizes $\sim 2.7\ \text{pc} \times 0.8\ \text{pc}$ and $\sim 1.8\ \text{pc} \times 1\ \text{pc}$) located at R.A. (J2000) = $14^{\text{h}}41^{\text{m}}23^{\text{s}}$ and Dec. (J2000) = $-64^{\circ}04'17''$ and R.A. (J2000) = $05^{\text{h}}05^{\text{m}}35^{\text{s}}$ and Dec. (J2000) = $-69^{\circ}35'25''$ were selected for the study. The difference in the average dust color temperatures calculated using IRIS and AKARI maps of the cavity candidates were found to be $3.2 \pm 0.9\ \text{K}$ and $4.1 \pm 1.2\ \text{K}$, respectively. Interestingly, the longer wavelength AKARI map gives larger values of dust color temperature than that of the shorter wavelength IRIS maps. Possible explanation of the results will be presented.

Keywords. ISM—dust—cavity—IRIS—AKARI.

1. Introduction

A variety of dust structures such as shells, cavities, lobes, filaments, arcs and loops have been discovered on Infrared Astronomical Satellite (IRAS) maps (Odenwald and Rickard 1987; Odenwald 1988; Weinberger and Armsdorfer 2004; Kiss *et al.* 2004; Aryal and Weinberger 2006; Koenyves *et al.* 2007; Aryal *et al.* 2009, 2010; Jha *et al.* 2017). The formation and evolution these structures are assumed to be ruled by the bubbles and superbubbles produced by high pressure events (Brand and Zealey 1975; Weaver *et al.* 1977; Aryal and Weinberger 2006). Therefore, these far infrared (FIR) dust structures usually considered to be a clear hints of interaction processes in the interstellar medium (ISM). The discovery of a very large ($\sim 9^{\circ}$) jet-like structures in the FIR (Weinberger and Armsdorfer 2004) suggest the interactions of the wind of the asymptotic giant branch (AGB) stars with ambient interstellar matter. Odenwald and Rickard (1987) and Odenwald (1988) performed a visual survey of IRAS maps in the $100\ \mu\text{m}$, discovered 15 high Galactic latitude clouds with comet-like appearance and discussed their FIR and optical properties. On 100 and $60\ \mu\text{m}$ IRAS maps, Aryal *et al.* (2010) found two giant (2.1 pc, 0.9 pc) bipolar dust emission structures centred on NGC 1514, representing one of

the very few known cases where the preserved history of all main mass-loss phases of a star of intermediate initial mass. These bipolar dust structures are slightly tilted with respect to each other due to precession. NGC 1514 is found to be least disturbed at $100\ \mu\text{m}$, which is of symmetrical shape, reminiscent of a bipolar outflow. Its length-to-width ratio is ~ 3 . A distinct peak of emission is present in the north, about 0.44 pc distant from NGC 1514.

Aryal *et al.* (2009) found that the planetary nebula (PN) NGC 2899 is located at the center of a huge ($14\ \text{pc} \times 11\ \text{pc}$) quadrupolar cavity, whose directions of axes coincide with the directions of the main axes of the optical PN. Aryal and Weinberger (2006) detected a new infrared nebula (R.A. = $08^{\text{h}}27^{\text{m}}$, Dec. = $+25^{\circ}54'$ (J2000)) with an apparent size of $\sim 140' \times 70'$ on $60\ \mu\text{m}$ and $100\ \mu\text{m}$ IRAS maps, suggested that the pulsar PSR B0823+26 might be responsible for its shaping.

Kiss *et al.* (2004) and Koenyves *et al.* (2007) identified 462 far-infrared loops (Kk-loops hereafter) at $60\ \mu\text{m}$ and $100\ \mu\text{m}$ IRAS maps, studied their far infrared properties and concluded that these structures are formed by supernovae and stellar winds. They suggested that these cavity-like dust structures might be formed due to the high-pressure events occurred in the

past (e.g., supernova explosion, stellar wind, etc.). AGB wind, pulsar wind, supersonic wind, etc., interact with ambient interstellar medium to form interstellar bubble, cavity and loops (Weaver *et al.* 1977).

Jha *et al.* (2017) studied dust color temperature, dust mass and inclination angle of core region of KK-loops, namely G007+18, G143+07, G214-01 and G323-02, in IRIS (Miville-Deschnes and Lagache 2005) maps. These loops are found to be located within 1° from pulsars PSR J1720-1633, PSR J0406+6138, PSR J0652-0142 and PSR J1535-5848, respectively. The dust color temperature of the core region of these loops is found to lie in the range $19.4 \pm 1.2 - 25.3 \pm 1.7$ K.

We intend to investigate new FIR loops or cavities similar to 462 far infrared loops (Kiss *et al.* 2004; Koenyves *et al.* 2007) in both IRIS (Miville-Deschnes and Lagache 2005) and AKARI (Murakami *et al.* 2007) maps and study their dust color temperature distributions. Our aim is to interpret the offset in the temperatures of the dust using $60 \mu\text{m}$ and $100 \mu\text{m}$ IRIS data and $90 \mu\text{m}$ and $140 \mu\text{m}$ AKARI data.

2. Cavities at IRIS and AKARI maps

We performed a systematic search around KK-loops in 60 and $100 \mu\text{m}$ IRIS maps to find similar FIR loops. The selection criteria were as follows: (1) loops should be isolated from KK-loops (at least 10° far from the KK-loops), (2) major diameter of the loop should be $> 0.5^\circ$, and (3) No optical diffuse emission (surface brightness limit $\sim 5 \text{ mag/arcsec}^2$ with resolution 2 arcsec, and size 1.7 sec/pixel) (Lasker *et al.* 1990). We found two loop-like dust cavities centered at R.A. (J2000) = $05^{\text{h}}05^{\text{m}}35^{\text{s}}$, Dec.(J2000) = $-69^\circ35'25''$ ($l = 280.7^\circ$ and $b = -34.4^\circ$) and R.A.(J2000) = $14^{\text{h}}41^{\text{m}}23^{\text{s}}$, Dec.(J2000) = $-64^\circ04'17''$ ($l = 314.6^\circ$ and $b = -03.7^\circ$) (figures 1a, 2a). These structures are found in AKARI maps (Murakami *et al.* 2007): WIDE-S band ($50-110 \mu\text{m}$, centred at $90 \mu\text{m}$) and the WIDE-L band ($110-180 \mu\text{m}$, centred at $140 \mu\text{m}$) (figures 1b, 2b). The reason for the selection of these two cavity-like structures are as follows: (1) both are elongated (eccentricity > 0.70) having similar position angle ($\sim 135^\circ$) and found in IRIS and AKARI, (2) almost equal in area (~ 600 square arcmin) in projected maps.

The FITS images of IRIS and AKARI maps are downloaded from IRSA interface (NASA/IPAC Infrared Science Archive) and SkyView Virtual Observatory (<http://skyview.gsfc.nasa.gov/current/>), respectively. IRIS maps benefit from better zodiacal emission

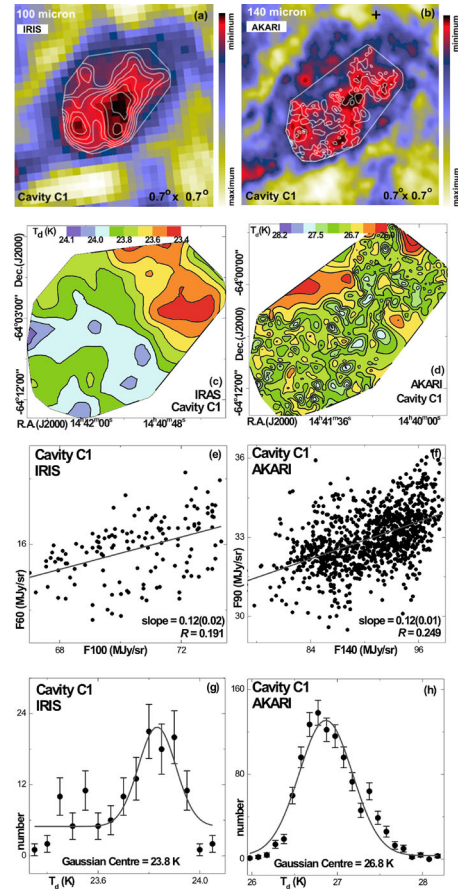


Figure 1. FIR image of cavity C1 at (a) $100 \mu\text{m}$ (IRIS) and (b) $140 \mu\text{m}$ (AKARI) maps, where contours represent $67.8, 68.6, 69.4, 70.2, 70.9, 71.7 \text{ MJy sr}^{-1}$ (a), and $78.9, 81.7, 84.6, 90.2 \text{ MJy sr}^{-1}$ (b), respectively. All fields are centred at R.A.(J2000) = $14^{\text{h}}41^{\text{m}}23^{\text{s}}$, Dec.(J2000) = $-64^\circ04'17''$. The dust color temperature map of cavity C1 using (c) IRIS data (60 and $100 \mu\text{m}$) and (d) AKARI data (90 and $140 \mu\text{m}$). The contour levels (step size 0.1 K) for dust color temperatures are shown. (e) $60 \mu\text{m}$ versus $100 \mu\text{m}$ and (f) $90 \mu\text{m}$ versus $140 \mu\text{m}$ plots. The values of slope and regression coefficient (R) are shown. The dust color temperature distribution in the region of interest (g, h). The $\pm 1\sigma$ statistical error bars are shown. The Gaussian fits (solid lines) are shown.

subtraction, calibration and zero-level compatible with COBE/ DIRBE, and better describing than that of the IRAS maps available at SkyView Virtual Observatory. The resolution and size of each pixel in the IRAS and AKARI are 2 arc min, 0.025 deg/pixel and 88 arc-sec, 44.1 sec/pixel , respectively (Miville-Deschnes and Lagache 2005; Takita *et al.* 2015).

The background emission is subtracted from the field using the method as adopted in Aryal *et al.* (2010). For this, we used surrounding regions where values of flux density is the lowest. The mean value of lowest flux density region is determined by making histogram. This

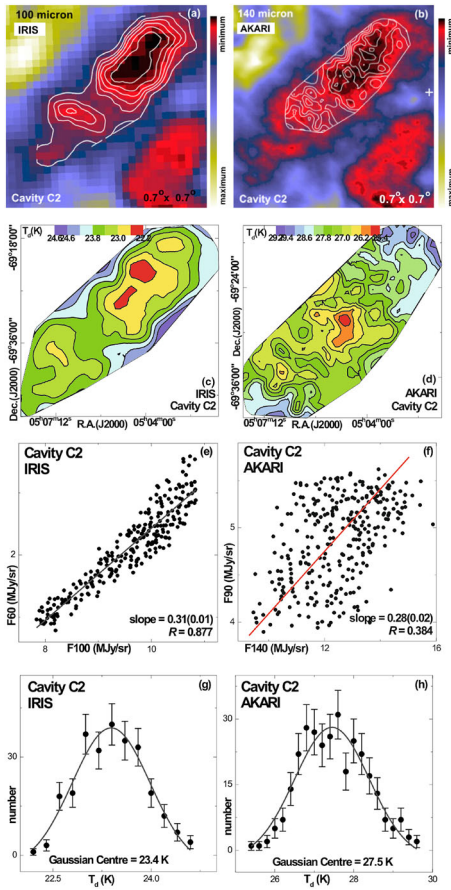


Figure 2. FIR image of cavity C2 at (a) 100 μm (IRIS) and (b) 140 μm (AKARI), where contours represent 7.8, 8.2, 8.6, 9.0, 9.3, 9.7 MJy sr⁻¹ (a), and 9.4, 10.2, 11.1, 11.9, 12.7, 13.5, 14.3, 15.1 MJy sr⁻¹ (b), respectively. All fields are centered at R.A.(J2000) = 05^h05^m35^s, Dec.(J2000) = -69°35'25". The dust color temperature map of cavity C2 using (c) IRIS data (60 and 100 μm) and (d) AKARI data (90 and 140 μm). The contour levels (step size 0.4K) for dust color maps are shown. (e) 60 μm versus 100 μm and (f) 90 μm versus 140 μm plots. The values of slope and regression coefficient (*R*) are shown. The dust color temperature distribution in the region of interest (g, h). The ±1σ statistical error bars are shown. The Gaussian fits (solid lines) are shown.

value is assumed to be the background and is subtracted from each pixel. The background correction has been made in both 60 and 100 μm IRIS and 90 and 140 μm AKARI maps. We use ALADIN2.5 software to get the values of flux density at each pixels from FITS image of the cavities C1 and C2. The foreground emission is also subtracted from the region by considering the flux density contributed by the nearby stars and IRAS sources. For this SIMBAD (<http://simbad.u-strasbg.fr/simbad/>) is used. Fig. 1a shows 0.7° × 0.7° 100 μm cavity-like IRIS structure (C1 hereafter) having major, minor diameters and position angles 46.4', 14.6' and

~136° ± 2°, respectively. The value of minimum flux density (67.1 MJy/sr) is found at R.A.(J2000) = 14^h41^m23^s, Dec.(J2000) = -64°04'17". Its mean value was 70.6 MJy/sr with standard deviation (sd) 1.67 (sde = 0.14). Fig. 1b shows AKARI WIDE-L (140 μm) map of the same field. In AKARI, the value of minimum flux density is found to be 76.1 MJy/sr with mean value 90.7 MJy/sr (sd = 4.5 MJy/sr, sde = 0.14). Therefore, as the wavelength increases from 100 μm to 140 μm, the mean values of flux density is found to increase by 22%. There are 137 and 1 077 pixels in IRIS and AKARI maps of the cavity C1, with pixel size 90 sec/pixel and 44.1 sec/pixel, respectively. Table 1 shows the values of minimum and maximum flux densities with mean, standard deviation and standard error for both cavities.

Fig. 2a shows 0.7° × 0.7° 100 μm cavity-like IRIS structures (C2 hereafter) having major, minor diameters and position angles 30.7', 18.0' and ~139° ± 2°, respectively. The flux density minima (7.83 MJy/sr) is found at R.A.(J2000) = 05^h05^m35^s, Dec.(J2000) = -69°35'25". AKARI WIDE-L (140 μm) map of the same field can be seen in Fig. 2b. In this cavity, the mean value of flux density is found to increase by 23% as the wavelength increases from 100 μm (IRIS) to 140 μm (AKARI). In the cavity C2, there are 260 and 408 pixels in IRIS and AKARI maps.

The errors given with dust color temperature (*T_d*) is mainly due to the variation in the background and foreground subtraction. The ±1σ errors in *T_d*-distribution and dust mass come from the variation between background and foreground emissions.

3. Dust color temperature distribution

Using the method developed by Dupac *et al.* (2003) and Schnee *et al.* (2005), we have calculated dust color temperature of each pixel in both cavities. The expression for the temperature is given by

$$T_d = \frac{-96}{\ln\{R \times 0.6^{(3+\beta)}\}}, \quad (1)$$

where

$$R = \frac{F(60 \mu\text{m})}{F(100 \mu\text{m})} \quad (2)$$

Here *F*(60 μm) and *F*(100 μm) are the flux densities at 60 μm and 100 μm respectively. The value of β depends on dust grain properties (e.g., composition, size, compactness, structure, etc). Its value is assumed to be zero for a perfect blackbody. The amorphous layer-lattice matter has β ~ 1, and the metals and crystalline dielectrics have β ~ 2.

Table 1. Values of flux densities in IRIS and AKARI maps of both cavities. The first three columns represent the cavity, survey and the wavelength.

Cavity	Survey	λ	F (min)	F (max)	\bar{F}	sd	se
		(μm)	(MJy/sr)	(MJy/sr)	(MJy/sr)	(MJy/sr)	(MJy/sr)
C1	IRIS	60	14.85	17.15	15.93	0.46	0.04
C1	IRIS	100	67.14	73.23	70.58	1.67	0.14
C1	AKARI	90	29.64	36.27	32.97	1.07	0.03
C1	AKARI	140	76.13	98.65	90.71	4.55	0.14
C2	IRIS	60	1.39	2.79	2.04	0.33	0.02
C2	IRIS	100	7.83	10.83	9.54	0.84	0.05
C2	AKARI	90	3.89	5.32	4.88	0.45	0.02
C2	AKARI	140	9.45	15.88	12.48	1.33	0.08

The next three columns shows the minimum, maximum and mean (\bar{F}) values of flux densities. The last two columns list the values of standard deviation (sd) and standard error (se)

Table 2. Minimum and maximum values of dust color temperature at IRIS and AKARI maps of cavities C1 and C2.

Cavity	Survey	T(min)	RA(J2000)	Dec.(J2000)	T(max)	RA(J2000)	Dec.(J2000)
		(K)	(hhmmss)	(ddmmss)	(K)	(hhmmss)	(ddmmss)
C1	IRIS	23.4	14 ^h 40 ^m 13.6 ^s	−64°01′59.9″	24.1	14 ^h 42 ^m 54.9 ^s	−64°05′53.5″
C1	AKARI	26.0	14 ^h 41 ^m 01.2 ^s	−63°56′58.4″	28.2	14 ^h 39 ^m 35.7 ^s	−63°59′52.4″
C2	IRIS	22.2	05 ^h 03 ^m 59.5 ^s	−69°23′49.3″	24.6	05 ^h 03 ^m 50.8 ^s	−69°37′12.5″
C2	AKARI	25.4	05 ^h 04 ^m 35.3 ^s	−69°28′26.8″	29.7	05 ^h 02 ^m 32.1 ^s	−69°17′01.7″

First two columns give the name of the cavity and FIR survey. The third column lists the minimum values of dust color temperature. The next two columns give the positions. The maximum values of dust color temperature and their positions are listed in last three columns

A good correlation is noticed when making plots between 60 μm versus 100 μm data in IRIS (figure 1e,f) and 90 μm versus 140 μm in AKARI (figure 2e,f) for both cavities. The slopes of best fitted lines are found to be similar in IRIS and AKARI. The presence of multiple temperature are removed by plotting and fitting flux densities of 60 μm versus 100 μm (or 90 μm versus 140 μm). Table 2 shows the minimum and maximum values of dust color temperature in the cavities C1 and C2. The dust color temperature of cavity C1 which is located close to the galactic plane ($b = -3^\circ$) is found to lie in the range 23.4 ± 1.3 K to 24.1 ± 1.4 K with an offset of only 0.7 K in IRIS maps. Narrower the range of T_d , higher the probability of being in the thermal equilibrium (Weinberger and Armsdorfer 2004), because the values of planck function is almost constant here. In the AKARI, the value of T_d is found to lie in the range 26.0 ± 1.5 K to 28.2 ± 1.6 K, with an offset of 2.2 K.

Here the temperature offset is found to be small, suggesting that the dusts in the cavity C1 are mostly in the thermal equilibrium. In other words, the mean free path of dusts and the reciprocal of absorption coefficient of FIR radiation is of the same order.

In the IRIS, the value of T_d for cavity C2, which is far from the galactic plane ($b = -34^\circ$), is found to lie in the range 22.2 ± 1.2 K to 24.6 ± 1.3 K, with an offset of about 2.4 K. In the AKARI, the value of T_d is found to lie in the range 25.4 ± 1.4 K to 29.7 ± 1.7 K, with a larger offset of 4.3 K. In the cavity C2, the difference is found to be 2.4 K in IRIS and 4.3 K in AKARI maps. This difference suggests that the values of planck function is not uniform in the cavity. Therefore, temperature may vary within the mean free path of the dust. This leads deviation from local thermodynamical equilibrium.

The difference between the value of average dust color temperatures at IRIS and AKARI is found to

be 3.2 ± 0.9 K and 4.1 ± 1.2 K in cavities C1 and C2, respectively. At longer wavelengths (AKARI), dust color temperature is found larger than in the shorter wavelength (IRIS) region. This is because of the presence of external cause that possibly drives the pressures in the field. These cavities may formed due to such events in the past.

In order to compare dust color temperature maps in IRIS and AKARI, we fix the contour levels at equal steps by fixing their temperatures using software ALADIN2.5. We set 0.1K for C1 (figure 1c,d) and 0.4K temperatures for C2 (figure 2c,d). In both cavities, the minimum temperature region is found to be shifted from the region of flux minima. This is interesting that the longer wavelength data (AKARI) yield higher temperature than that of the IRIS, the shorter wavelength. Higher the temperature, the collisional frequencies between dust–dust, dust–grain and grain–grain increases (Aryal and Weinberger 2006). This causes a systematic changes in the matter distribution.

Figs. 1g, h and 2g,h show the T_d -distribution in IRIS and AKARI maps of C1 and C2, respectively. These distributions fit well with the Gaussian, suggesting that the structure is now relaxing and self-evolving, and seems to be isolated.

Figs. 3a, b shows the T_d distribution along the major diameters (east to west) of the cavities C1 and C2 in both IRIS and AKARI maps. The statistical parameters are shown. Interestingly, the value of T_d is found to be greater in both AKARI maps. The difference in the average T_d calculated using IRIS and AKARI along the major diameters of C1 and C2 are found to be 3.3 ± 0.9 K and 4.5 ± 1.2 K, respectively. A fluctuation in longer wavelength (AKARI) map is noticed (figure 3b).

4. Inclination angle

The long axis of dust cavities can be assumed to be inclined by a certain angle with respect to the plane of the sky. The inclination angle i (angle between the line-of-sight and the normal vector of the plane of the loops) can be estimated using Holmberg (1946) formula:

$$\cos^2 i = \frac{(b/a)^2 - q^2}{(1 - q^2)} \quad (3)$$

where b/a is the measured axial ratio and q is the intrinsic flatness of the cavity. Since we have the database of diameters of four loops we determine their inclination angles. We use the value of intrinsic flatness $q = 0.33$

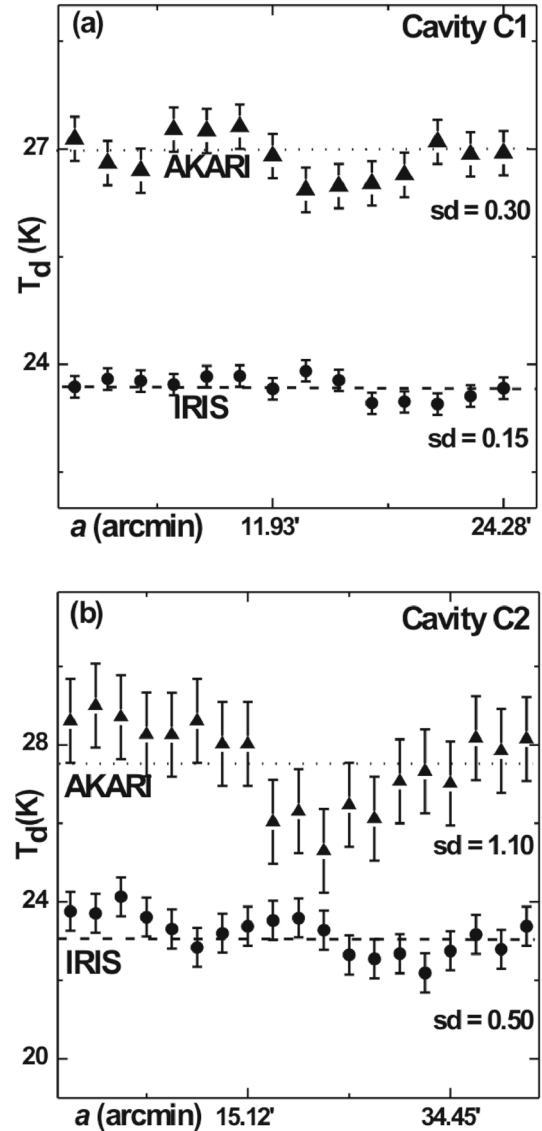


Figure 3. Dust color temperature variation along the major diameters passing through minima at $100 \mu\text{m}$ (IRIS) and $140 \mu\text{m}$ (AKARI) maps for cavity (a) C1 and (b) C2. The observed values with $\pm 1\sigma$ statistical error bars are shown. The dashed lines represent mean value. The standard deviations are shown. Interestingly the dust color temperature is found to be more when using $140 \mu\text{m}$ and $90 \mu\text{m}$ data of AKARI maps in both cavities.

as suggested by Holmberg (1946) for oblate spheroid structure.

It can be assumed that the long axis of cavities C1 and C2 are inclined by a certain angle with respect to the plane of the sky. The inclination angle (i) of cavities C1 and C2 are found to be $\sim 56^\circ$ and $\sim 76^\circ$, respectively. It means that our dusty cavity is neither face-on ($i \rightarrow 0^\circ$) nor edge-on ($i \rightarrow 90^\circ$) object. The C1 will be face-on (minor axis / major axis ~ 0.20 , $i = 0^\circ$) if we rotate it

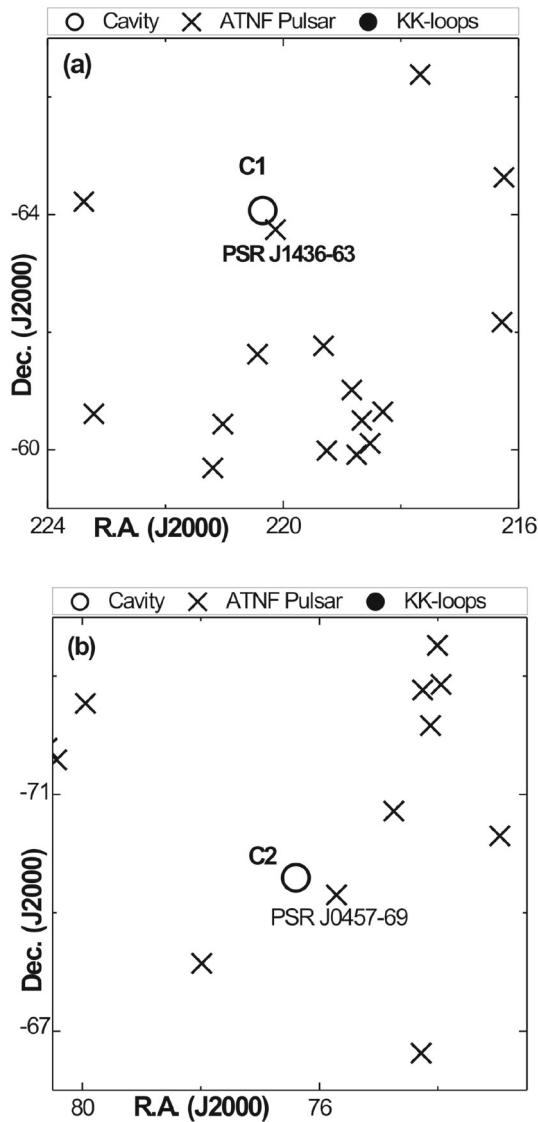


Figure 4. Discrete sources in the field of cavity C1 and C2. ATNF pulsars PSR 1436-63 (a) and PSR J0457-69 (b) are found within 0.5° from the centre of the cavities C1 and C2. The symbols (\times) represent the ATNF pulsars.

by ~ 34 (i.e.) from the northern to the southern direction (assuming that the cavity is in the sky plane). Similarly, the cavity C2 will be face-on (minor diameter / major diameter ~ 0.20 , $i = 0^\circ$) if we rotate it by $\sim 14^\circ$ (i.e.) from the northern to the southern direction (assuming that the cavity is in the sky plane).

5. Discrete sources around cavities

We searched for ATNF pulsars which might be capable of forming cavity within 8° radius from the centre of the cavity. There were 16 and 12 pulsars (figure 4).

The nearest pulsars were PSR J1436-63 and PSR J0457-69, located $< 0.5^\circ$ from the centre of the cavities C1 and C2. The distance to the pulsars are not available in the ATNF catalog. While searching for a nearby source within 0.5° using SIMBA D, we found two additional possible candidates around cavity C1, planetary nebula (PN) G314.8-03.6 and PN G314.3-03.4. These objects are found to be associated with dust. In order to estimate physical size of the cavity, 200 pc distance is assumed as a reference, as suggested by Odenwald and Rickard (1987) for $100 \mu\text{m}$ dust. Using this, the size of the cavity C1 is found to be $2.7 \text{ pc} \times 0.7 \text{ pc}$.

Similarly, we found four additional possible candidates around cavity C2, namely two post AGB stars (2MASS J05055 872-6939538 and SSTITAGEMC J050633.28-694015.9) and a planetary nebula ([RP2006] J050600-692830) within 0.5° radius. Using 200 pc distance, the size of the cavity C2 is found to be $1.8 \text{ pc} \times 1.0 \text{ pc}$.

In the future, we intend to find out the reason for the formation and evolution of these FIR cavities. In addition, we intend to work on KK-loops which are located very close to the pulsar, AGB stars and white dwarfs.

6. Conclusion

A systematic search of similar cavity-like structures was carried out in the far-infrared ($60 \mu\text{m}$ and $100 \mu\text{m}$) IRIS and AKARI ($90 \mu\text{m}$ and $140 \mu\text{m}$) surveys. The physical properties (dust color temperature, inclination, etc.) of these dust structures are studied.

The dust color temperature of cavity C1 and C2 in IRIS is found to lie in the range $23.4 \pm 1.3 \text{ K}$ to $24.1 \pm 1.4 \text{ K}$ and $22.2 \pm 1.2 \text{ K}$ to $24.6 \pm 1.3 \text{ K}$, with an offset of about 0.7 K and 2.4 K , respectively. In the AKARI, the dust color temperatures are found to lie in the range $26.0 \pm 1.5 \text{ K}$ to $28.1 \pm 1.6 \text{ K}$ and $25.4 \pm 1.4 \text{ K}$ to $29.7 \pm 1.7 \text{ K}$, with an offset of about 2.1 K and 4.3 K , in the cavities C1 and C2 respectively. The difference in the values of T_d is found to be less than a few kelvin temperature. This suggests that the planck function is almost constant in the region, indicating dusts in the cavities are mostly in the thermal equilibrium.

The difference between the value of average dust color temperatures at IRIS and AKARI is found to be $3.2 \pm 0.9 \text{ K}$ and $4.1 \pm 1.2 \text{ K}$ in cavities C1 and C2, respectively. At longer wavelengths (AKARI), dust color temperature is found larger than in the shorter

wavelength (IRIS) region. This is probably because of the high-pressure events occurred in the past.

The size of the cavity C1 and C2 are found to be $\sim 46.4' \times 14.6'$ and $\sim 30.7' \times 18.0'$, located at R.A. (J2000) = $14^h 41^m 23^s$ and Dec. (J2000) = $-64^\circ 04' 17''$ and R.A. (J2000) = $05^h 05^m 35^s$ and Dec. (J2000) = $-69^\circ 35' 25''$. Its physical size is of the order of $\sim 2.7 \text{ pc} \times 0.8 \text{ pc}$ and $\sim 1.8 \text{ pc} \times 1 \text{ pc}$, assuming 200 pc distance as a reference (Odelwald & Rickard 1987).

The inclination angle (i) of the cavity C1 and C2 are found to be 76° and 56° respectively, suggesting that the cavities will be face-on ($i = 0^\circ$) if it is rotated by 14° and 34° from northern to southern direction (assuming the cavities are in the sky plane).

This is the first work in this series. We intend to work on the formation and evolution of FIR loops including 462 KK-loops.

Acknowledgements

We are indebted to the referee for his/her constructive criticism and useful comments. We acknowledge SIMBAD database, Sky View Virtual Observatory and NASA/IPAC Infrared Science Archive. One of the authors (AKJ) acknowledges Central Department of Physics, Tribhuvan University, Nepal for all kinds of support for his research work.

References

- Aryal B., Weinberger R. 2006, A&A, 44, 1, 213
 Aryal B., Rajbahak C., Weinberger R. 2009, Ap&SS, 323, 323
 Aryal B., Rajbahak C., Weinberger R. 2010, MNRAS, 402, 1307
 Brand P. W. J. L., Zealey W. J. 1975, A&A, 38, 363
 Dupac X., Bernard J.-P., Boudet N., Giard M., Lamarre J.-M. et al. 2003, A&A, 404, L11
 Kiss Cs., Mor A., Tth L. V. 2004, A&A, 418, 131
 Koenyves V., Kiss Cs., Mor A., Kiss Z. T., Tth L. V. 2007, A&A, 463, 3, 1227
 Lasker B. M., Sturch C. R., McLean B. J., Russell J. L., Jenkner H., Shara M. M. 1990, AJ, 99, 2019
 Jha A. K., Aryal B., Weinberger R. 2017, RMxAA, 53, 467
 Miville-Deschênes M. A., Lagache G. 2005, Astrophys. J. Suppl. Ser., 157, 2, 302
 Murakami H., Baba S., Barthel P., Clements D. L., Cohen M., Doi Y., Enya K. et al. 2007, Publ. Astron. Soc. Japan 59, S369
 Odenwald S. F. 1988, ApJ, 325, 320
 Odenwald S. F., Rickard L.J. 1987, ApJ, 318, 702
 Schnee S. L., Ridge N. A., Goodman A. A., Jason G. L. 2005, ApJ, 634, 442
 Takita S., Doi Y., Ootsubo T., Arimatsu K., Ikeda N., Kawada M., Kitamura Y. et al. 2015, PASJ, 67, 3, 51
 Weaver R., McCray R., Castor J., Shapiro P., Moore R. 1977, ApJ, 218, 377
 Weinberger R., Armsdorfer B. 2004, A&A, 416, L27